22

A SIMPLIFIED MODEL FOR THE STUDY OF SMOKE PLUME DISPERSION FROM GRASSFIRES AND A METHODOLOGY FOR FORECASTS VALIDATION WITH SATELLITE IMAGES

Joaquin E. Blanco * and Guillermo J. Berri #

Servicio Meteorologico Nacional, Argentina
Member of Consejo Nacional de Investigaciones Científicas y Técnicas (CONICET), Argentina

ABSTRACT

The purpose of this work is to present the smoke plume dispersion model HIRHYLTAD (HIgh-Resolution HYbrid Lagrangian Trajectory and Atmospheric Dispersion), and a methodology for an objective validation of smoke plume forecasts, with high resolution imagery from AQUA and TERRA satellites. Two meteorological models are used as input for HIRHYLTAD, the operational regional Eta/SMN model from the Argentine Servicio Meteorológico Nacional (SMN), and the Mesoscale Boundary Layer Model (MBLM), which was especially developed for the La Plata River region. The smoke plume forecasts are performed with the HIRHYLTAD puff model, which is based on the Gaussian model. It first determines smoke lines using lagrangian trajectories, an then simulates dispersion and calculates concentrations. The model uses the Pasquill stability classes, the Pasquill-Gifford dispersion coefficients according to the stability class, and the Briggs scheme for buoyant plume rise. The advantage of HIRHYLTAD in comparison with other dispersion models widely used, is that it requires minimum data, i.e. wind, temperature and cloudiness, so that computational costs are significantly reduced. The methodology for this work includes adjustments of satellite images, digitization of smoke plumes, definition and selection of smoke events, determination of number of smoke sources for each event, and definition of initial and final time of emission for each source. Different indices with simple and direct interpretation are employed for the validation: the Plume Overlay Area Error index (POAE), and the Plume Mean Orientation Error index (PMOE). The reason for including these two indices is that each one measures a different property of the smoke distribution.

1. INTRODUCTION

Forest and grassland fires are responsible for the deterioration of ecosystems, often the recovery may require several decades, and they also have a major impact on population and social activities. Every year in Argentina a variable number of wildfires take place especially during summer over dry regions, and in occasions they are due to prescribed burnings in rural zones, which become uncontrolled and remain so for several days.

This study focuses on the smoke produced by pasture burnings that took place during April and May 2008 in the Paraná River Delta, some 70 km to the northwest of the city of Buenos Aires. The smoke however, propagated over wide regions according to the prevailing atmospheric conditions for each day. Smoke spread hundreds of kilometers across the La Plata River, towards northeast into Uruguay and southern Brazil, and as far south as the extreme south of Buenos Aires province. The grassfires burnt out about 70,000 hectares in the provinces of Buenos Aires and Entre Ríos (a map of the study region can be seen in Fig. 1).

Within that period, an extreme event without historical precedent occurred during 16 to 20 April 2008 affecting the city of Buenos Aires and its suburbs, with an approximate population of 13 million people. Fig. 2a and Fig. 2b illustrate the situation for the afternoon of April 16 and 18, in which an extensive burning area in southern Entre Ríos province originated a dense smoke plume that propagated to Buenos Aires and the La Plata River. Fig. 2c shows the extensive smoke area extending across Buenos Aires province and the La Plata

* Corresponding author address: Joaquin E. Blanco, Servicio Meteorológico Nacional, 25 de mayo 658, Buenos Aires, Argentina.
E-mail: joaquin_eb@hotmail.com

River, associated to a wind rotation, for April 20 in the morning.

The episode resulted in an increase of health problems among the population (respiratory problems, eye irritation, etc.). Due to visibility reduction, there were hazardous driving conditions and accidents that forced the intermittent closure of freeways, as well as the inoperability of airports. During those days, the persistence of anomalous northwesterly winds contributed to that situation, which under normal conditions for that time of the year would have not occurred. Such impact was reflected in the fact that the event was the main issue addressed by local and regional media, even capturing international attention as well.

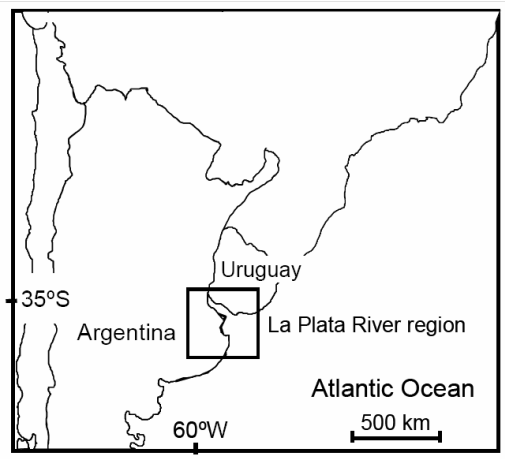

Figure 1: Location of La Plata River region in South America.

Marcuzzi and Hoevel (2009) studied the prevailing weather conditions in the region during the events and previous days. Otero et al (2009) analyzed observations of Atmospheric Optical Thickness (AOT) and the Angstrom exponent for the CEILAP-CIFEFA station located near the city of Buenos Aires. Mattio (2009) analyzed the detection and evolution of fire outbreaks, and performed simulations of smoke concentrations with HYSPLIT dispersion model coupled to global (GFS) and regional (Eta/SMN) meteorological models with intermediate resolution (1º and 30km respectively). The authors validated the plumes only qualitatively, by means of a direct comparison against plume distribution in the MODIS images.

Berbery et al (2008) studied the period from 15 to 20 April using the WRF-ARW regional model at a grid spacing of 6 km and performed a 5-day simulation in both diagnostic and forecast modes. The authors focused mainly on the predictability of the smoke episode, in terms of the effects of local dynamics such as the river-land breeze and atmospheric boundary layer processes. In fact, they explain the channeling effect of the low-level atmospheric circulation in the La Plata River on the observed smoke plume during April 18, as it spread out in southeasterly direction (see Figure 2b), although no smoke plume simulations were made.

In the following section we present the HIRHYLTAD model, which was used to perform smoke plume simulations during the entire episode (April 1 – May 15). It was coupled to different meteorological models to account for the effects of different scale processes (section 3). Data and methodology are described in section 4; in particular, new error indices to quantitatively validate these forecasts are presented. Finally, Section 5 describes the study results, followed by the summary and conclusion of this work (section 6).

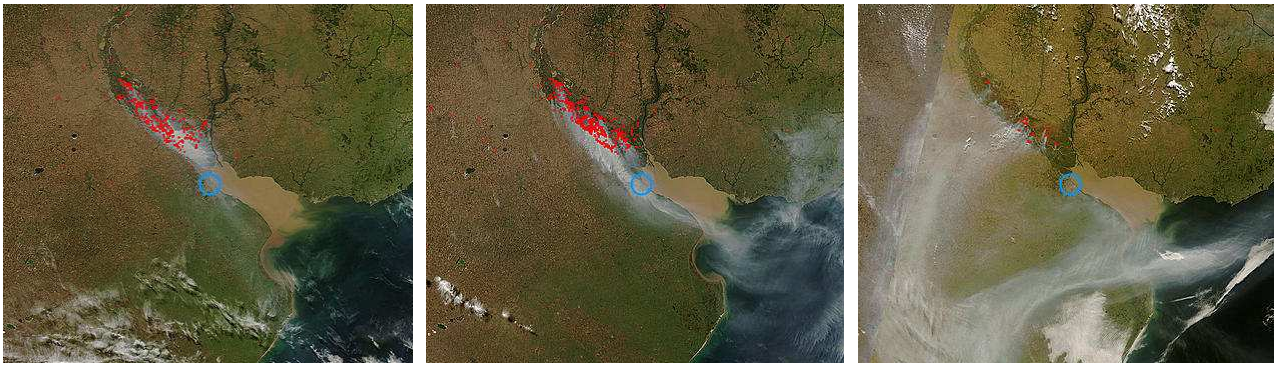

Figure 2: MODIS real-color images (CEILAP-BA subset) from: a) AQUA, April 16 at 18.00 UTC; b) AQUA, April 18 at 17.50 UTC; c) TERRA, April 20 at 15.00 UTC. Red dots correspond to MODIS automated fire detections. The blue circle indicates the location of the city of Buenos Aires.

2. THE HIRHYLTAD DISPERSION MODEL

2.a. Model overview

On the basis of a pre-existing smoke line algorithm (Berri, 2009) a new simplified dispersion model was created using the Gaussian theory. HIRHYLTAD (Blanco and Berri, 2010) is hybrid because in the smoke line model the input is a forecasted wind field at discrete time intervals, while the Gaussian model assumes homogeneous and stationary conditions, as well as continuity. Moreover, it is hybrid because it uses a Lagrangian coordinate system (mobile) to calculate the trajectories of individual elements of the smoke plume, and an Eulerian framework (fixed) to calculate concentrations in a high resolution grid.

The adaptation of the Gaussian model (scheme depicted in Fig. 3) to obtain HIRHYLTAD can be summarized in the following pair of equations. The Gaussian equation is given by:

$$C(x,y,z) = \frac{Q}{2\pi u \sigma_y \sigma_z} \exp\left(\frac{-y^2}{2\sigma_y^{\,2}}\right)\left[\exp\left(\frac{-(z-H)^2}{2\sigma_z^{\,2}}\right)\right]$$

where σ_y and σ_z, were parameterized by Pasquill (1961) and Gifford (1976), based on Pasquill's stability classes.

The actual equation used by HIRHYLTAD is given by:

$$C_{i,j}(t) = \frac{Q}{2\pi \bar{u}(t)\sigma_{y\#}(t)\sigma_z(t)} \exp\left(\frac{-y_\#^{\,2}}{2\sigma_{y\#}^{\,2}(t)}\right)\exp\left(\frac{-(z-H(t))^2}{2\sigma_z^{\,2}(t)}\right)$$

Naturally, several differences arise between them. New dependence on time of most parameters (H, u, σ), natural coordinates fixed to the plume axis (x#,y#) replace Cartesian coordinates (x,y) (although a Cartesian coordinate system is used for the concentrations), and calculated concentration is now on discrete (i,j) grid points, and for t=kΔt time intervals.

A special treatment of Pasquill-Gifford equations for σ_y and σ_z, was carried out to account for transition from stable to unstable stratification (or vice versa). Also, eventual singularities that might come up during the simulation are solved, such as $\bar{u}(t) = 0$ or $\sigma_{y\#}(t), \sigma_z(t) = 0$.

The plume rise for the effective emission height (left panel in Fig. 3) is parameterized using the scheme from Briggs (1972). Sensitivity tests for Δh, as well as for other parameters were performed to calibrate the model (not shown).

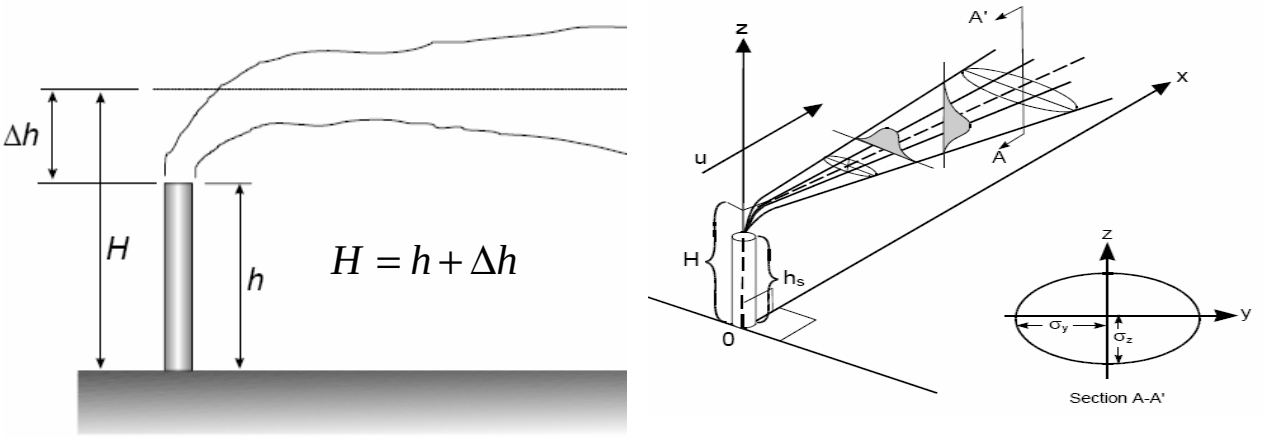

Figure 3: Left: Emission heights. Δh is the buoyant plume rise, which summed to the physical emission height (h) gives the effective emission height (H). For stack emissions Δh is calculated using Briggs parameterization. Right: The idealized plume from the Gaussian model, which uses Pasquill-Gifford dispersion coefficients to set values for σ_y and σ_z,. These two, dependent of Pasquill stability classes, not only determine the size of each puff (as depicted above) but also the concentration on it.

Fig. 4 provides a basic scheme of the operations performed by HIRHYLTAD. The main application of this model is on small-scale high-resolution dispersion simulations, for varied phenomena such as stack emissions from factories (model originally developed for this purpose) and smoke plumes originated by grassfires or forest fires. It can be used either as a research tool for case studies (diagnostic mode) or to perform operational forecasts.

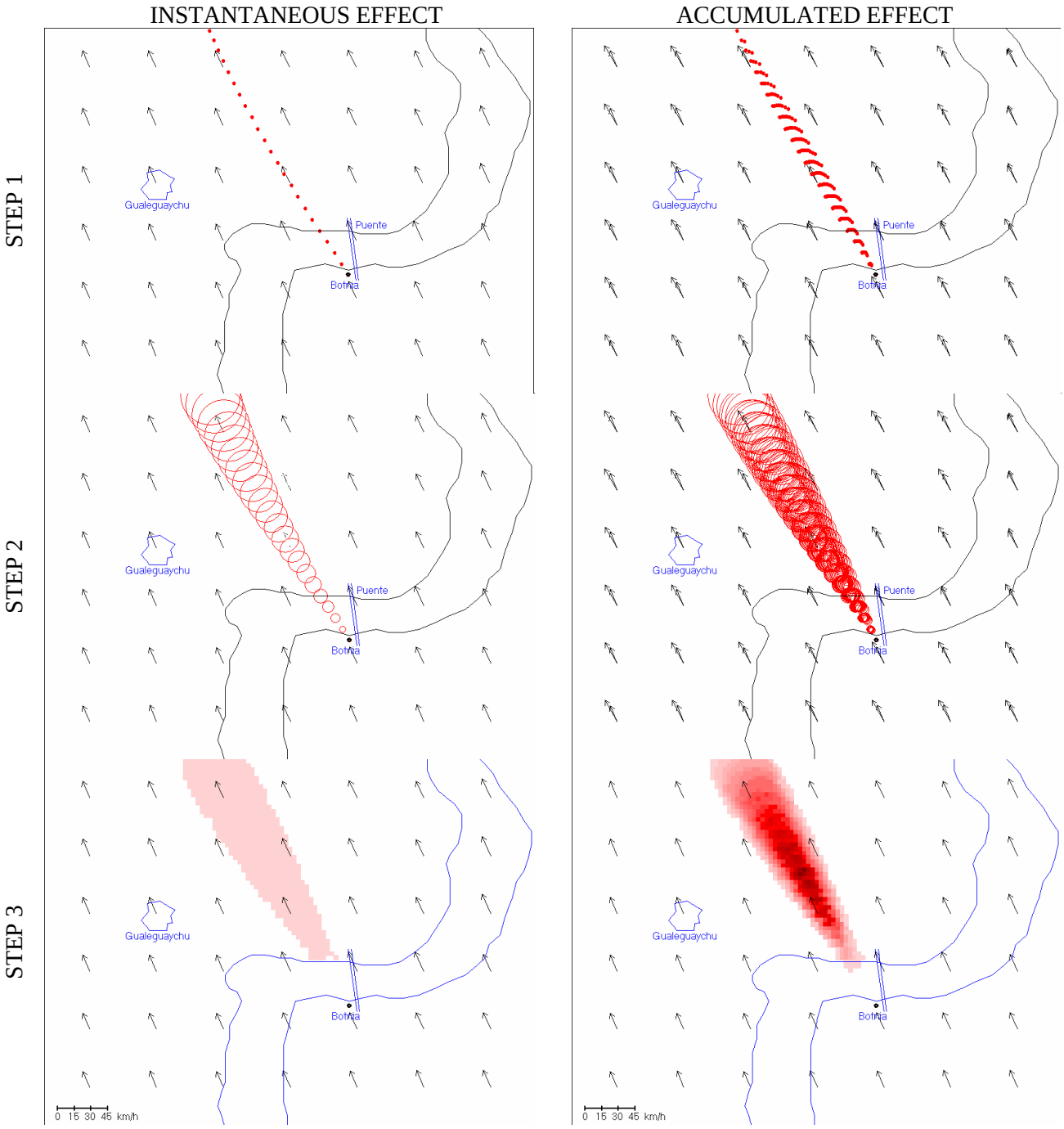

Figure 4: Overview of the HIRHYLTAD model. Top (step 1): Smoke line setting-up using Lagrangian trajectories. Center (step 2): Smoke puffs in the horizontal, with Pasquill-Gifford dispersion coefficients and Pasquill stability classes. Bottom (step 3): Smoke concentrations on a high resolution grid, either for a specified z-level or vertically integrated. The instantaneous (accumulated) effect can be seen on the left (right) column. Figures were obtained after a 2-hour simulation, showing 24 smoke line elements/puffs (model time step = 5 min). Panels in step 3 show surface concentrations. The physical emission height in these simulations was 120 m.

HIRHYLTAD has some advantages, in comparison with other dispersion models widely used; for example, it requires minimum data (only wind, temperature and cloudiness), it is easily coupled to a meteorological model, and reduces computational costs (in terms of process time and disk space).

2.b. Adapted version for smoke plume simulations

Several changes were introduced in order to apply the HIRHYLTAD model to smoke dispersion simulations originated by grassfires. Unlike simulations for stack emissions, smoke sources are variable in location and number, depending

on the particular situation. Also, as the Pasquill stability class is calculated for every grid point at each time step of the simulation using an algorithm based on a land surface, a correction is imposed in the case of a water surface (as in the La Plata River, and Uruguay and Paraná Rivers), using a relaxed shift of the stability class, either stable or unstable, toward the neutral case.

There is an important issue regarding the Briggs scheme, which was originally developed for stack emissions. It requires the setting of 3 main parameters at each time step, associated with the source emission: smoke temperature *Ts* and vertical velocity *ws* at its origin, and the 'effective' diameter of the smoke column *Ds*. Since no direct measurements were available for the simulations performed in the Paraná River Delta events, results from the FireFlux grassfire field experiment (Clements et al, 2007) were used. Hence, simplified constant values of *Ts* = 200º C. and *ws* = 1m/s were used for all simulations, regardless of the grass burning intensity or fuel consumption. To be consistent with those values, the smoke initial height was considered to be 10m instead of the surface level, so that $H(t) = 10m + \Delta h(t)$. To set a unique value for *Ds*, a sensitivity test was performed, and it was found that *Ds* = 2.5m (larger than a typical stack diameter, but with the same order of magnitude) was the most appropriate. Under this assumption, Δh oscillates between 50 and 150m for stable conditions, and ranges between 250m and 350m for neutral and unstable conditions. The instantaneous value that Δh might take also depends on the ambient wind speed.

3. METEOROLOGICAL MODELS AND EXPERIMENTS

3.a. Meteorological Models

Two meteorological models are used as input for HIRHYLTAD, the operational regional Eta/SMN model from the Argentine Servicio Meteorológico Nacional (SMN), and the Mesoscale Boundary Layer Model (MBLM) especially designed for the La Plata River region.

The MBLM, developed by Berri in 1987 is a primitive equation, dry and hydrostatic model, with a high definition of the water-land temperature gradient. The horizontal resolution is 0.05º, which corresponds to an average of 5km. The vertical domain has 12 levels distributed according to a log-linear spacing. The first level is the roughness length z_0 (equal to 0.0001m over water and 0.01m over land), and the last one is the material top of the model at 2000m. The intermediate levels are located at the following heights: 10, 40, 80, 140, 220, 350, 550, 800, 1100 and 1500 m. The upper boundary condition includes the geostrophic wind and temperature at the top of the model. These data can either be taken from local radiosonde observations, or from regional model outputs. At this level, pressure and temperature perturbations as well as vertical wind, are set equal to zero. The lower boundary condition consists of $u=v=w=0$, and the definition of a surface heating function as follows:

$$T(x,y,t) = T_0 + F_1(t)F_2(x,y)$$

where T_0 is a mean temperature, $F_1(t)$ defines the daily cycle of the maximum river-land temperature difference, and $F_2(x,y)$ defines the river-land temperature difference as a function of the distance between every (x,y) point and the coast. Except near the coast, the horizontal air temperature gradients over the land and over the river are small. Again, model inputs for setting $F_1(t)$ come either from observational data or larger-scale model outputs. Above the surface layer (z>40m), the prognostic equations are solved by a semi-implicit numerical scheme. Within the constant-flux layer, the forecasts equations become diagnostic equations by applying the similarity theory, and therefore reduce to logarithmic vertical profiles of wind and temperature, as a function of stability. The MBLM is initialized under conditions of horizontal homogeneity for all the variables, except for pressure, since its gradient defines geostrophic wind at the initial state (for more details please refer to Berri et al, 2010).

The Eta Model is a state-of-the-art atmospheric model used for research and operational purposes, developed in the seventies in the former Yugoslavia by Mesinger and Janjic. In the eighties, the code has been upgraded to the Arakawa-style horizontal advection scheme of Janjic, then rewritten to use the eta vertical coordinate, and subsequently, at NCEP, supplied with an advanced physics package (details of the Eta model can be found at Mesinger, 1984; Mesinger and Janjic, 1990; Black, 1994).

The regional Eta/SMN model was implemented at the SMN in 2002, after an adaptive process for the South American region. The horizontal domain corresponds to 30º-91º W and 14º-65º S, with grid spacing of 1/3 º (approx. 30 km), and a rotated spherical coordinate system is used. The boundary and initial conditions are provided by the GFS model, and it runs in a hydrostatic mode, for 38 hydrostatic pressure levels in the vertical. The model is operationally run twice a day (00 UTC and 12 UTC) performing 120-hour forecasts at 3-hour intervals.

3.b. Experiment Design

A set of 6 experiments was performed. The first two were carried out using the Eta/SMN model outputs: these correspond to diagnostic and prognostic modes (EXP 1A and EXP 1B). EXP 1A consists of the usage of the first 24-hour forecast period, from successive model runs; a temporal interpolation was made between the forecast at hour +24 and the analysis of the consecutive run, with a higher weight for the analysis. Horizontal, vertical and temporal interpolations of Eta/SMN outputs to MBLM resolution were required to perform plume simulations with HIRHYLTAD in small spatial and temporal scales.

The remaining 4 experiments were conducted with the MBLM. As in the case of the Eta/SMN model, diagnostic and prognostic modes were performed, and also for two types of initialization: observations (EXP 2 A and B, respectively) and outputs from the Eta/SMN model (EXP 3 A and B respectively).

The MBLM was run for a 24-hour period in all cases, starting at 12 UTC or 09 local standard time (LST), approximately 2-3 hours after sunrise, when there is a minimum land-river temperature contrast. This forecast is taken after 30 min of model integration, in order to facilitate the model spin-up. As the MBLM is a dry model, cloudiness for stability calculation in these 4 experiments was taken from the Eta/SMN outputs.

For the experiments with observations, the input for lower boundary condition consists of surface temperatures at 03, 09, 15 and 21 LST from the weather stations Ezeiza (located 40 km southwest of the city of Buenos Aires), and Pontón Recalada (lightship on the La Plata River, 30 km off the coast). The forcing at the upper boundary was taken from the 12 UTC 1000-hpa level Ezeiza radiosonde sounding. Since this observation is the only one available for the whole MBLM domain (which in turn, is approximately in its center point), homogeneous conditions are considered for the geostrophic wind at the top of the model. In the case of diagnostic mode (EXP 2A), two observations (hour 0 and hour +24) are used in the model run, with temporal interpolation along the integration period. In the prognostic mode (EXP 2B), data are assimilated only at the beginning so that the upper boundary condition remains stationary.

In a similar way, EXP 3A and 3B use analysis and forecasts from Eta/SMN outputs at two grid points only: one over land (nearest grid point to Ezeiza station) and the other over water (approximately at the center of the La Plata River). Data assimilation for these two experiments occur at initialization and every 6 hours.

4. DATA AND METHODOLOGY

4.a. Data

High resolution imagery from AQUA and TERRA satellites are used, which are equipped with the Moderate-Resolution Imaging Spectroradiometer (MODIS) instrument. True-color images (one per day for each satellite) are available from the MODIS Rapid Response System (MRRS) at NASA/GSFC. The AERONET_CEILAP-BA subset is used (centered in the La Plata River region), as it best covers the affected region of study. Coordinates for the 965 km x 720 km domain are: 63.7º-53.2º W, 31.3º-37.8º S. This dataset of images is the most appropriate one from all available, for the study of local scale atmospheric phenomena such as smoke dispersion in the boundary layer.

The length of the period of analysis was determined not only through the direct visualization of smoke distribution in visible satellite images, but also by analyzing fire locations from automated detection algorithms with geostationary and polar-orbiting satellites. In this last case, two datasets were used: the Global Fire Maps from the MRRS (all MODIS detections in maps at 10-day intervals), and the ‘Banco de Dados Queimadas’ from CPTEC-

INPE, Brazil (more than 20 satellites intervening, including MODIS-equipped TERRA and AQUA's). The left panel of Fig. 5 depicts the distribution of the 5813 detections by different satellites between April 1 and May 15 in the Paraná Delta River region, as from the Brazilian fire dataset. Most of them occurred in the subperiod from April 14 to April 26, as it can be seen on the right panel. The 45-day period from April 1 and May 15 was finally chosen.

MODIS imagery constitute the only dataset to detect smoke events; a preliminary analysis was performed through GOES-12 imagery with higher temporal availability (data refresh of 15 min), but results were unsatisfactory mainly due to their lower resolution (1km visible, 4km infrared) and overall quality.

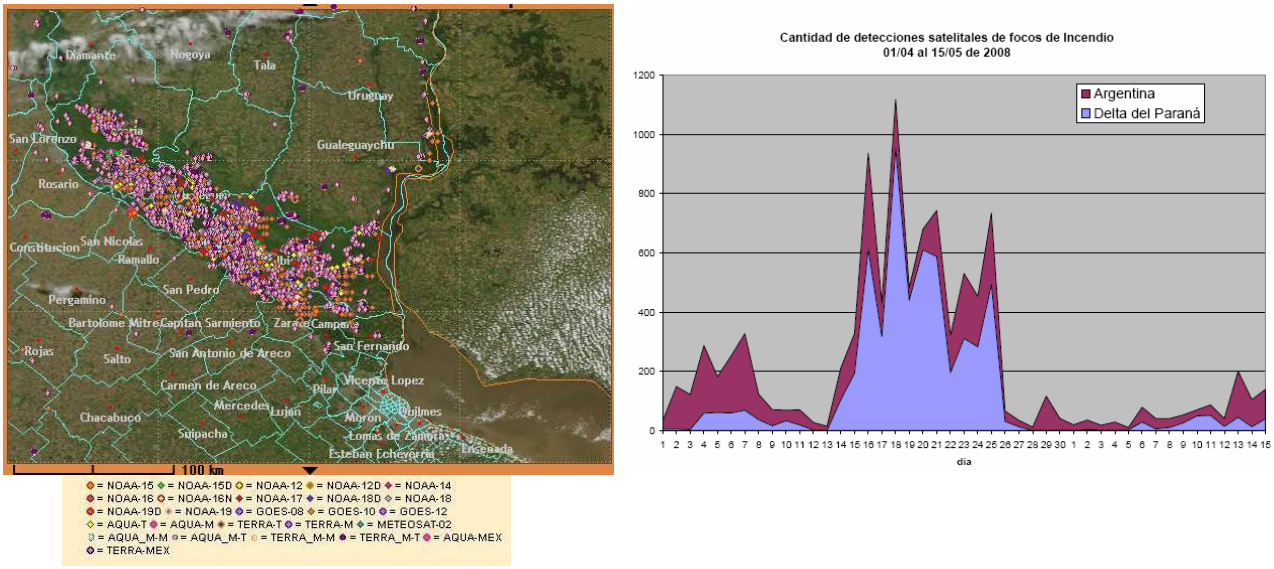

Figure 5: Left: Distribution of fire detections between April 1 and May 15 in the Paraná Delta River region. Pixel color according to the satellite, as indicated below. Right: Frequency histogram of fire detactions for the same period and satellites, in the Paraná Delta River region and in all Argentine territory. Data source: Banco de Dados Queimadas (CPTEC-INPE, Brazil).

4.b. Selection of smoke events and digitization

Real color 500m-resolution images from TERRA and AQUA were systematically adjusted for the period, totaling 90 images. The domain was reduced to a smaller-scale one, focusing on the La Plata River region (see panel on the left of Fig. 6), with an extension of 467 km x 500 km.

The process of selection of smoke events and digitization is completely subjective. For the selection of events, three particular cases were discarded: no smoke, cloudiness in excess, and sufficiently dispersed smoke with no clear source and/or source outside the domain (Fig. 6, right). A smoke event is defined as one in which a smoke plume is clearly identifiable with at least one associated fire location within the domain. The smoke plume can surpass the domain limits. More than one smoke event per image can be selected in case there were significant differences between the plume distributions (in amplitude, length and/or orientation).

A total of 21 events were selected from TERRA (from 18 days), and 38 from AQUA images (from 31 days) in the 45-day period of analysis. In no case, more than two events per image were selected. The smoke outlines are produced manually, and digitized using the ImageJ digital-image processing program; no quantitative estimate of the smoke concentration is used in the process. The reason for the larger number of AQUA events in comparison to TERRA events, could be the time of the day. The AQUA satellite overpasses the La Plata River region during the afternoon (in the band 1400-1600 LST) while TERRA does it during the morning (1000-1200 LST), when the fires (most of them intentionally produced) are starting to develop, yet not favored by the afternoon's higher temperatures.

Digitization of smoke sources was also accomplished, and it was found that multiple-fire-plumes were common, especially during the uncontrolled fires between April 16-20. The maximum number of fire locations detected in a single smoke event was 18. The analysis resulted in a total of 165 smoke sources for all the events from AQUA and 103 for TERRA's. Out of the 59 events, 21 are single-source while 38 multiple-source smoke plumes. The subjective methodology for determining smoke sources replaced the aforementioned MODIS automated fire detection product, since several cases of false detections and no detections were observed. An example of this process is depicted in Fig. 7.

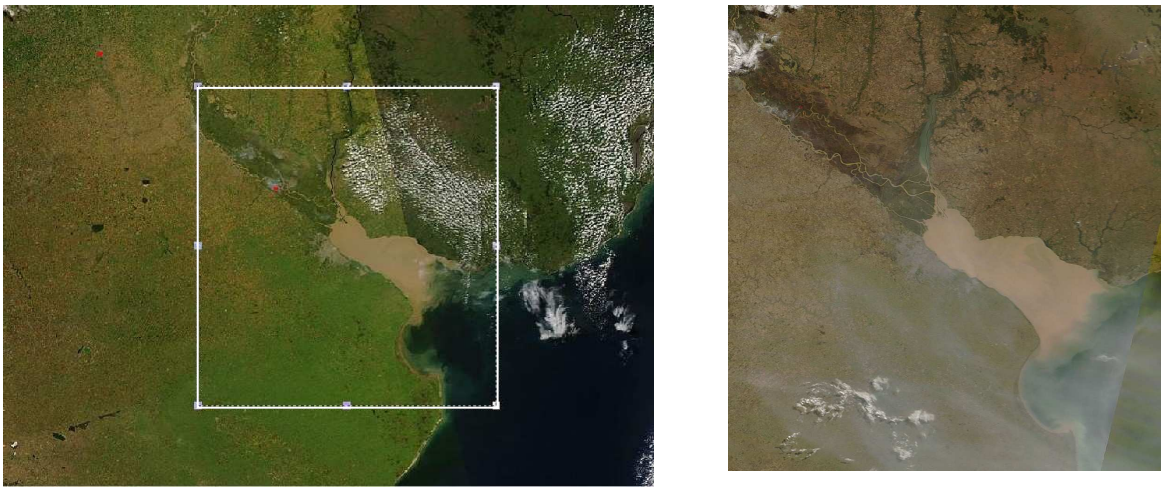

Figure 6: Left: Original MODIS satellite image from the AERONET-CEILAP subset, and domain of analysis indicated with a with box. Right: Example of no selection of smoke event in the MODIS adjusted image, because of the lack of a well-defined smoke source.

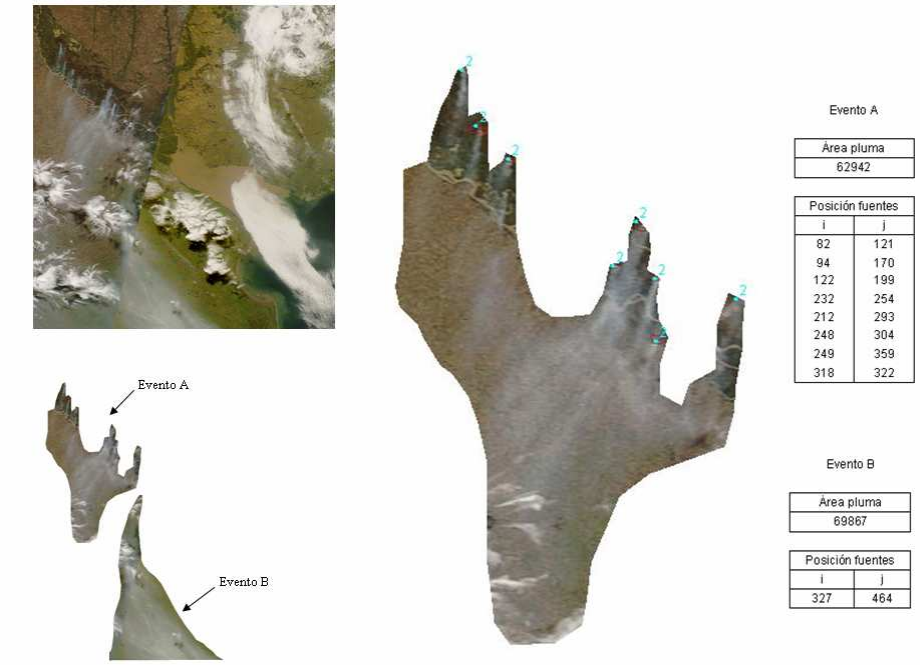

Figure 7: Example of 2 events per image: Left top: Adjusted MODIS image from satellite AQUA on 04/22/2008. Left bottom: Digitized A (multiple-fire plume) and B (single-fire plume) events. Center: Zoom on smoke event B with location of its 8 fire positions (light-blue dots). Right: Tables showing digitized locations of smoke sources for each event.

4.c. Smoke plume simulation

Smoke simulations were performed with the HIRHYLTAD model coupled to each of the 6 meteorological experiments, for the 59 smoke events. One of the main inputs was the digitized fire sources described above. In fact, multiple-fire plumes were obtained after individual simulations for each source, followed by the sum of their respective contributions of concentrations. The end time for simulations was determined from the metadata file associated to each MODIS image (also available online).

The start time for simulation and emissions represents a key issue in this analysis. The 'objective method' consisting of animation of successive satellite images with high temporal and spatial resolution to determine the onset of each fire spot could not been achieved, due to the lack of a complete and appropriate dataset. Visible GOES-12 imagery, unavailable during the nocturnal period, also have several gaps of missing data during diurnal hours. Although this methodology may have been applied to some particular events, a systematic analysis for all cases was not possible to develop. Hence, a subjective approach was used, consisting of an iterative process of HIRHYLTAD simulations until the length of a simulated plume best fits the length of the observed one, regardless of its direction of propagation. This method has some disadvantages. First, any meteorological model used in the simulation may imply a larger (smaller) duration for the event respect to another simulation from a different model, due to weaker (more intense) forecast winds. Even in the case of perfect agreement among all experiments, they all could be overestimating or underestimating the real duration of the event. Secondly, it affects validation, mainly through minimizing the errors regarding areas of intersection between observed and forecast plumes.

As a further consequence of lacking of adequate data, there was no basis for specifying fire duration, so that during the entire simulation, each fire source was supposed to be active. Additionally, each simulated source in HIRHYLTAD emitted at a constant rate of Q = 1 gr/s.

The threshold for setting the simulated plume boundaries was set equal zero: i.e., pixels with any positive value of smoke concentration are considered as part of the plume.

4.d. Validation

The verification analysis is based on the NOAA Smoke Forecasting System (SFS), comprising 3 parts: observation, prediction and validation of smoke plumes. Descriptions of these components can be found in Rolph et al (2009) and Ruminski et al (2006, 2007), while SFS products are available in real time at http://www.arl.noaa.gov/smoke.php.

Since compatibility of data formats between observed and forecast plumes is required, the first step consists on the conversion of the digitized pixel positions for all events onto the 5-km-resolution grid used by HIRHYLTAD. Two types of error are considered: errors in area and errors in direction of propagation.

Before introducing area errors, it is convenient to define area types. The areas of both observed and forecast plume shapes (*Aobs* and *Afor*) determine three other areas, namely: intersection or matching area (*Aint*), false detection area (*Afal*), and no detection area (*Anod*), as it can be seen in Fig. 8 and Fig. 9. The sum of these three areas corresponds to the union area (*Auni*).

The SFS uses the Figure of Merit in Space statistic, defined as the ratio of the intersection to the union of the plume areas

$$FMS = \frac{Aobs \cap Afor}{Aobs \cup Afor} = \frac{Aint}{Auni}.$$

This index can be rewritten as

$$FMS = \frac{Aint}{Aobs + Afor - Aint}.$$

FMS scores can range between 0 (no match at all) and 1 (ideal case, match for all pixels). Another statistical methods used by the SFS (and in this work) to measure the overlap area of the two shapes is the two-dimensional Measure of Effectiveness, defined as:

$$MOE(x, y) = \left(\frac{Aint}{Aobs}, \frac{Aint}{Afor} \right)$$

which can be rewritten as:

$$MOE(x,y)=\left(1-\frac{Anod}{Aobs},1-\frac{Afal}{Afor}\right).$$

Scores for all analyzed events can be plotted in a single x-y diagram.

The most visible limitation of these indices that consider the shape matching approach, is that their scores are often too low. This indicates apparently much poorer performances than what might be suggested by a qualitative examination of the spatial distribution of both observed and forecast plumes on a same image; the explanation lies on the nature of the *FMS* and *MOE* ratios. For this reason, Blanco and Berri (2010) defined a variant of *FMS*, called Plume Overlay Area Hit index, which is obtained by summing *Aint* in the numerator and denominator:

$$POAH=\frac{2Aint}{Aobs+Afor}.$$

Conceptually identical to *FMS*, this index not only ranges from 0 to 1 in the extremes, but also it shows a better performance for all intermediate cases, since $POAH \geq FMS$, as it can be easily demonstrated. If errors are to be accounted for, then the Plume for-no-Overlay Area Error index can be defined, subtracting *POAH* from unity:

$$POAE=1-\frac{2Aint}{Aobs+Afor}.$$

When *POAH*=1 then *POAE*=0 and vice versa.

Another type of validation that also improves the display of results in terms of meteorological and dispersion model performance, is the direction of propagation. The Plume Mean Orientation Hit index (Blanco et al, 2010) is defined as:

$$PMOH=1-\frac{\left|\overline{dir}_{obs}-\overline{dir}_{for}\right|}{180^{o}}$$

where $\overline{dir}_{obs}, \overline{dir}_{for}$ range from 0º to 360º, and the correction $\left|\left|\overline{dir}_{obs}-\overline{dir}_{for}\right|-360^{o}\right|$ replaces the numerator in case that $\left|\overline{dir}_{obs}-\overline{dir}_{pro}\right|>180^{o}$. The best possible score for the index is 1, if both mean directions are equal, and 0 if they are opposite (180º difference). Again, the error alternative of this index can be defined:

$$PMOE=\frac{\left|\overline{dir}_{obs}-\overline{dir}_{for}\right|}{180^{o}}.$$

For obtaining the mean direction of propagation, the equation used for the case of a single-source is

$$\overline{dir}=\arctan\left(\frac{\bar{j}-j_{source}}{\bar{i}-i_{source}}\right)$$

where $(\bar{i},\bar{j})$ correspond to the centroid position of the plume, and (i_{source}, j_{source}) are the (x,y) coordinates of the fire location.

In case of a multiple-source plume, the $(\overline{i_{source}}, \overline{j_{source}})$ coordinates are determined and then used in the previous equation. Other algorithms for the calculation of $\overline{dir}$ were also considered, but this approach was finally adopted.

The main advantage of the *PMOH* index against area indices such as *FMS* or *POAH*, can be seen in Fig. 8 and Fig. 9. In the first of the two examples (Fig. 8, for a single-source plume), while the area errors are of around 50% or worse, the *PMOE* is less than 5%, more in agreement with a straightforward appreciation of the two plume layouts. In contrast, in the following case for a multiple-source plume (Fig. 9), a 50% score for *POAE* index is not really representative of the model performance, as the forecast plume is propagating in opposite direction with respect to the observed plume, so that *PMOE* is near 100%.

5. RESULTS

As a qualitative example of the validation process, Fig. 10 depicts graphical results of the 6 experiments for one event, each accompanied by their respective area an direction error scores.

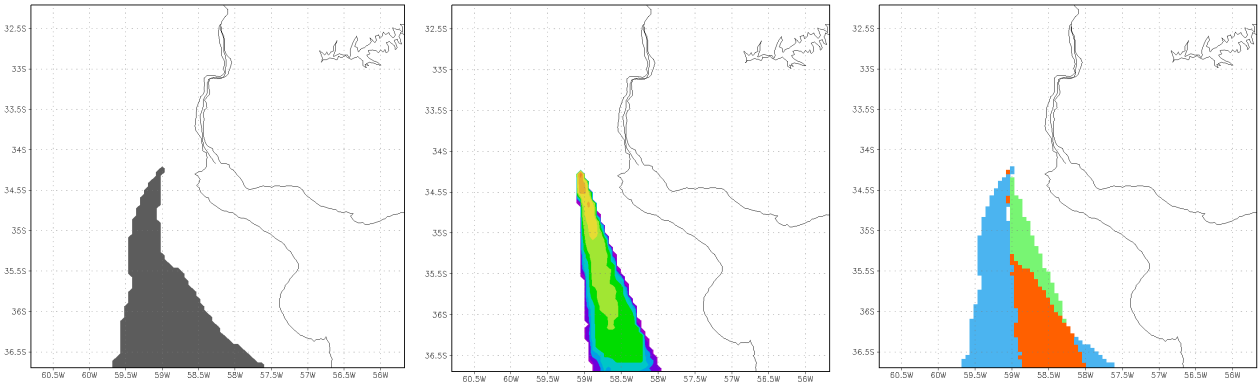

Figure 8: Left: digitized plume. Center: HIRHYLTAD output, where reddish color is indicative of higher concentrations. Right: Overlay, no detection and false detection areas are depicted in red, blue and green colors, respectively. Scores for area and direction error indices are: 1-FMS = 66.56%; POAE = 49.88%; PMOE = 4.34%.

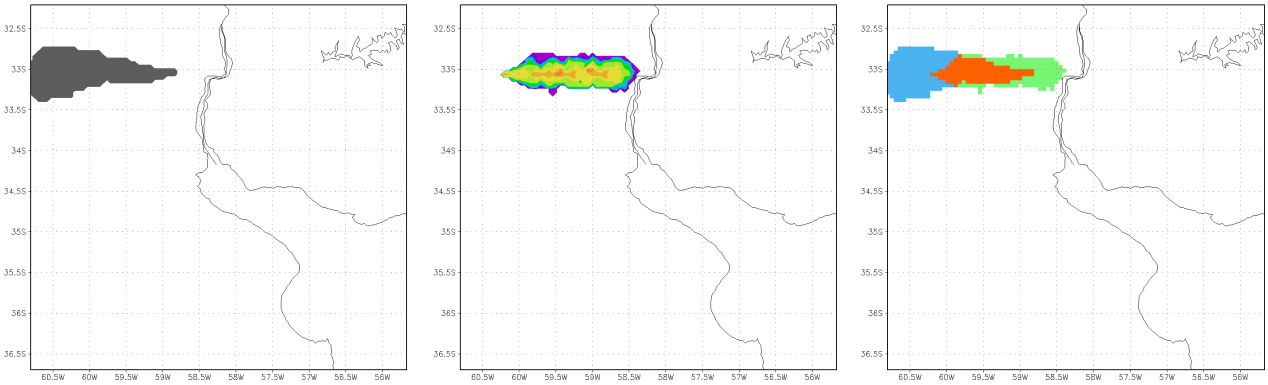

Figure 9: As Figure 8. Scores for area and direction error indices as follow:
1-FMS = 71.85 %; POAE = 56.07%; PMOE = 96.52%.

The advantage of defining an alternative area index and a new direction index can be appreciated in Fig. 11. Lower error scores are always obtained with *POAE* in comparison with the original *1-FMS*, as indicated before. But it is highly remarkable in this graphic the low *PMOE* scores for all events (red bars): except for one case, there were not errors in direction higher than 40% in the Experiment 1A simulations, and for 71% of the events (42 out of 59), error in direction was less than 10%.

Results for the 59 analyzed events for the 45-day period considered, show a better overall performance of forecasts obtained with the Eta/SMN model over both versions of the MBLM model, as basic statistics indicate (see Table 1). Best verification results were obtained with the diagnose mode (EXP 1A), in which the *POAE* index has scores of less than 47%, while the scores for the *PMOE* index are less than 9 %, for both median and average.

EXPERIMENT		**Area Error *POAE (%)***		**Direction Error *PMOE (%)***	
		Median	**Arithmetic mean**	**Median**	**Arithmetic mean**
1: Eta/SMN	A: Diag	43.5	46.6	7.3	8.6
	B: Prog	46.9	51.0	7.2	11.1
2: MCLM/obs	A: Diag	63.8	61.4	11.3	17.9
	B: Prog	58.5	59.7	11.4	19.9
3: MCLM/EtaSMN	A: Diag	59.7	59.2	10.5	17.8
	B: Prog	62.4	56.8	9.8	18.1

Table 1: Error scores of POAE and PMOE indices, for the 6 experiments performed.

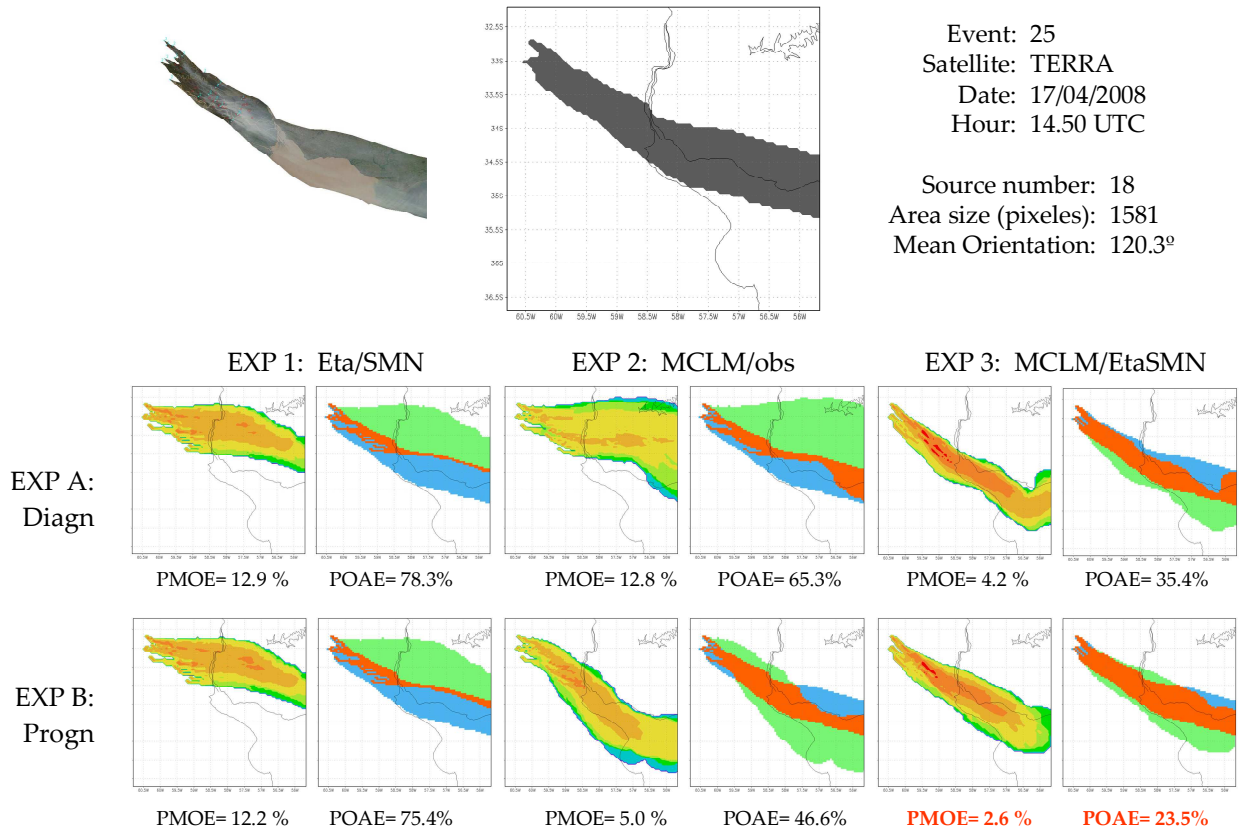

Figure 10: Example of graphical results of the validation process for event nº25. Top: Cropped smoke plume from the adjusted MODIS image (left), its corresponding digitized image (center), and details of the event (right). Bottom: Double-entry table showing smoke plume simulations from HIRHYLTAD (left) and area diagrams (right) for each of the 6 experiments. Colors of the dispersion model outputs, as well as in the area analysis, as in Figures 8 and 9. Below each pair of figures, the scores for both area and direction error indices are detailed; red color font highlights the experiment of best performance, i.e., EXP 3B with lowest scores.

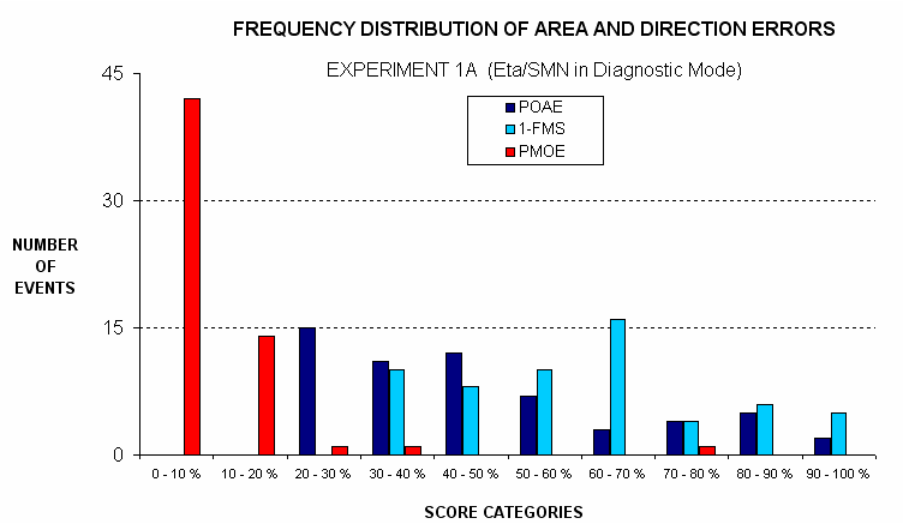

Figure 11: Frequency distribution of area (*POEA*, *1-FMS*) and direction (*PMOE*) errors for EXP 1A.

In order to intercompare the different experiments, the amount of best performances of each of the 59 events can also be used as a proper indicator. As seen in Fig. 12, again, there is an overall bad performance with the MBLM model (EXPs 2 and 3).

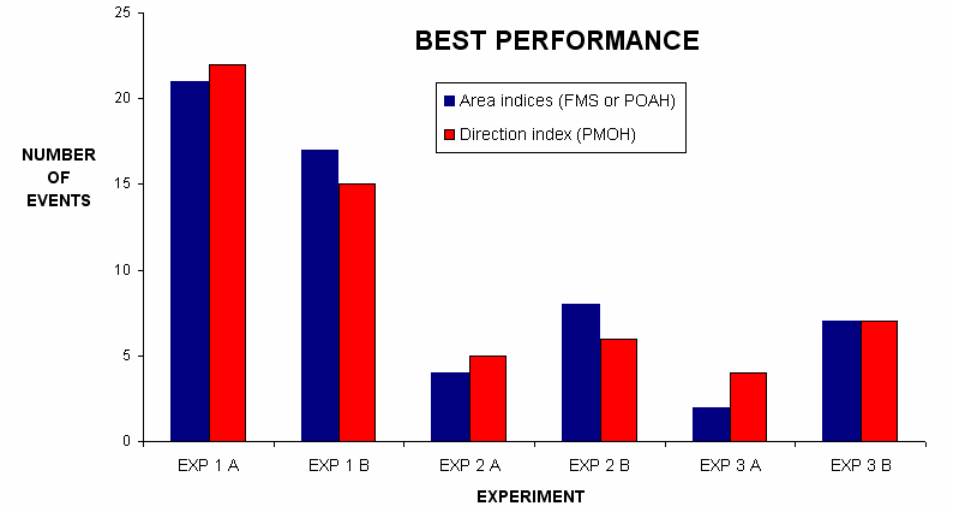

Figure 12: Each experiment contributes in a percentage to the total of events (59). For example, event nº25 (see Figure 10) contributes to the total number of best performances of EXP 3B, in both area an direction indices.

The reason for this situation can be found in the experiment design. As described in section 3, the MBLM meteorological model focuses mainly on the mesoscale phenomena associated to surface inhomogeneities, but the synoptic-scale forcing at the boundary layer top is rather simplified (homogenous geostrophic wind). In Fig. 13, a low-level wind field pattern from each model is depicted. It can be seen that, while the region Eta/SMN model is unable to reproduce the river-land breeze, in contrast with the MBLM, the latter cannot reproduce synoptic-scale wind shifts across its domain, unlike the former. For smoke plume dispersion over sufficiently long distances, the smaller-scale effects are not determinant.

The fact that in many cases with EXP 2, the prognostic mode shows better results over the diagnostic mode (as shown in Fig. 12 and Table 1) is also related to the previous analysis of synoptic scale representation. In this case, the key factor is a poor representation of the temporal (rather than spatial) variability within this scale. In the diagnostic mode, two observations (hour 0 and hour +24) of the 12 UTC radiosonde sounding are involved in the model run, with simple linear interpolation along the integration period. As changes in the atmosphere do not necessarily occur in a smooth and gradual way, the sounding at hour +24 can be very unrepresentative of the actual conditions even a few hours before (i.e.: at hour +18 or +21, for instance).

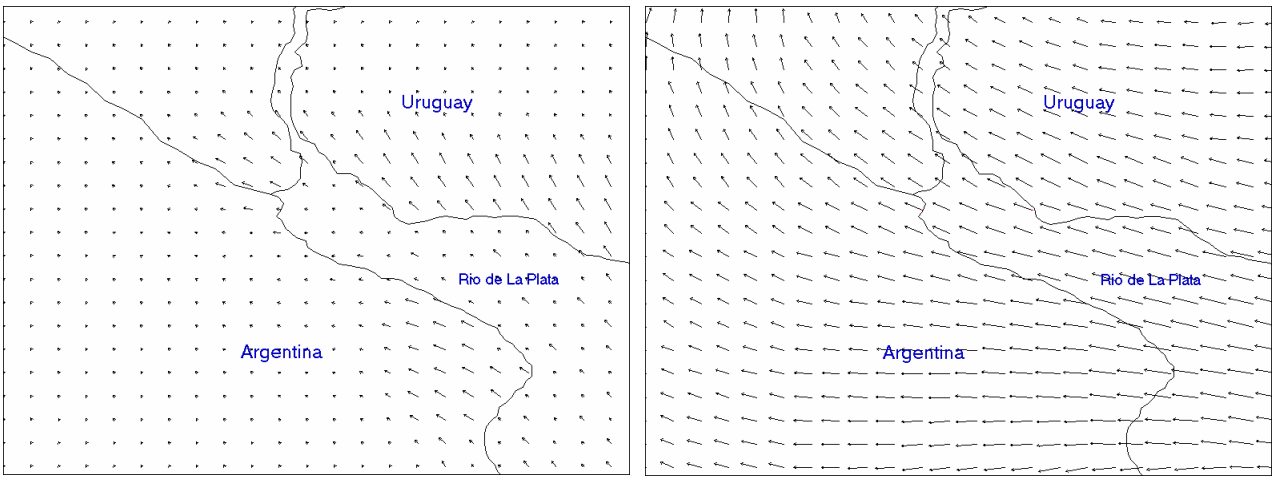

Figure 13: Examples of low level wind patterns obtained with the MBLM model (left) and the Eta/SMN model (right), in the La Plata River region, for different meteorological situations.

6. DISCUSSION AND CONCLUSIONS

This work introduces the HIRHYLTAD dispersion model, and new indices for validation of smoke plume forecasts originated by grassfires using high resolution imagery from AQUA and TERRA satellites. Table 2 summarizes the relative importance of factors that affect errors (indices' scores) of this study.

Factor	Relative importance
Meteorological model	Low
Experiment design	High
Dispersion model	Low
Methodology	High

Table 2: Factors that affect errors and degree of incidence, for this study.

While the experiments with the MBLM model showed a general bad performance, it is important to point out that with a more appropriate initialization in terms of the upper level wind, and a more frequent data assimilation, results would have undoubtedly been of similar or even better quality than with the Eta/SMN model. Accurate forecasts, from either global, regional or mesoscale models have obviously a high degree of incidence in plume simulations. This study suggests that a fair initialization and assimilation schemes during the model run are the real key factors rather than good model physics and dynamics. In fact, a stronger coupling of the MBLM to the Eta/CPTEC model (in which the nesting was for the entire grid, not a single point in the center of the domain) was achieved by Sraibman and Berri (2009), obtaining very good results.

The HIRHYLTAD model was used to simulate the smoke plumes, which were then compared with the observed events. Although simplified in terms of the parameterization of the horizontal puff dispersion rates (based on discrete stability classes via the Pasquill-Gifford equations), this dispersion model offered an acceptable performance for this study's purposes. Furthermore, a more complex dispersion model could not have been readily used (or may have not been as helpful as it could), as it demands not only more meteorological data but also input data associated with fire and emissions, which were unavailable for the studied events.

The methodology used in this work did influence significantly the results obtained in the previous section. Specifically, the subjective determination of start time of the simulation (duration of the event) implied both dependence on meteorological model and also error minimization. Also, there was no automated algorithm used for the smoke depiction from MODIS images; all of the smoke outline areas were manually derived (this procedure is also performed by the Hazard Mapping System from the NOAA's SFS).

Objective selection and validation of events with thresholds using Aerosol Optical Thickness (AOT) derived from MODIS were not performed, after the results of a preliminary analysis. Two reasons supported this decision: the lower resolution of this variable (resulting in incorrect low AOT values for high concentrated smoke near the source) and the abundance of missing data pixels (due to algorithm deficiencies); this last shortcoming was attempted to overcome using an interpolation scheme. An example is shown in Fig. 14, for one of the 'best events'; only the missing data problem was present in this case.

The verification indices presented in this work turned out to be very convenient for the displaying of results, not only because they score better for the same analysis (as the case of area indices: POAH vs FMS), but also because they together provide a better insight of the pair observed-forecasted plume (PMOH direction index vs overlay area indices). It was shown that sometimes an area index does not really represent the validation results, but the new direction index does. Moreover, these indices can be used with different meteorological models, dispersion models and methodologies (selection of events, simulations settings, thresholds).

Finally it is worth to mention that since 2009, the HIRHYLTAD model (coupled to the regional Eta/SMN model) is operationally run at the SMN to produce 72-hour smoke plume forecasts emitted from the stack of a paper pulp mill factory in the bordering city of Fray Bentos, Uruguay (location and domain are depicted in Fig. 4). There is a joint agreement between the SMN and the Secretary of Environment and Sustainable Development, to assist in an environmental monitoring program in the region.

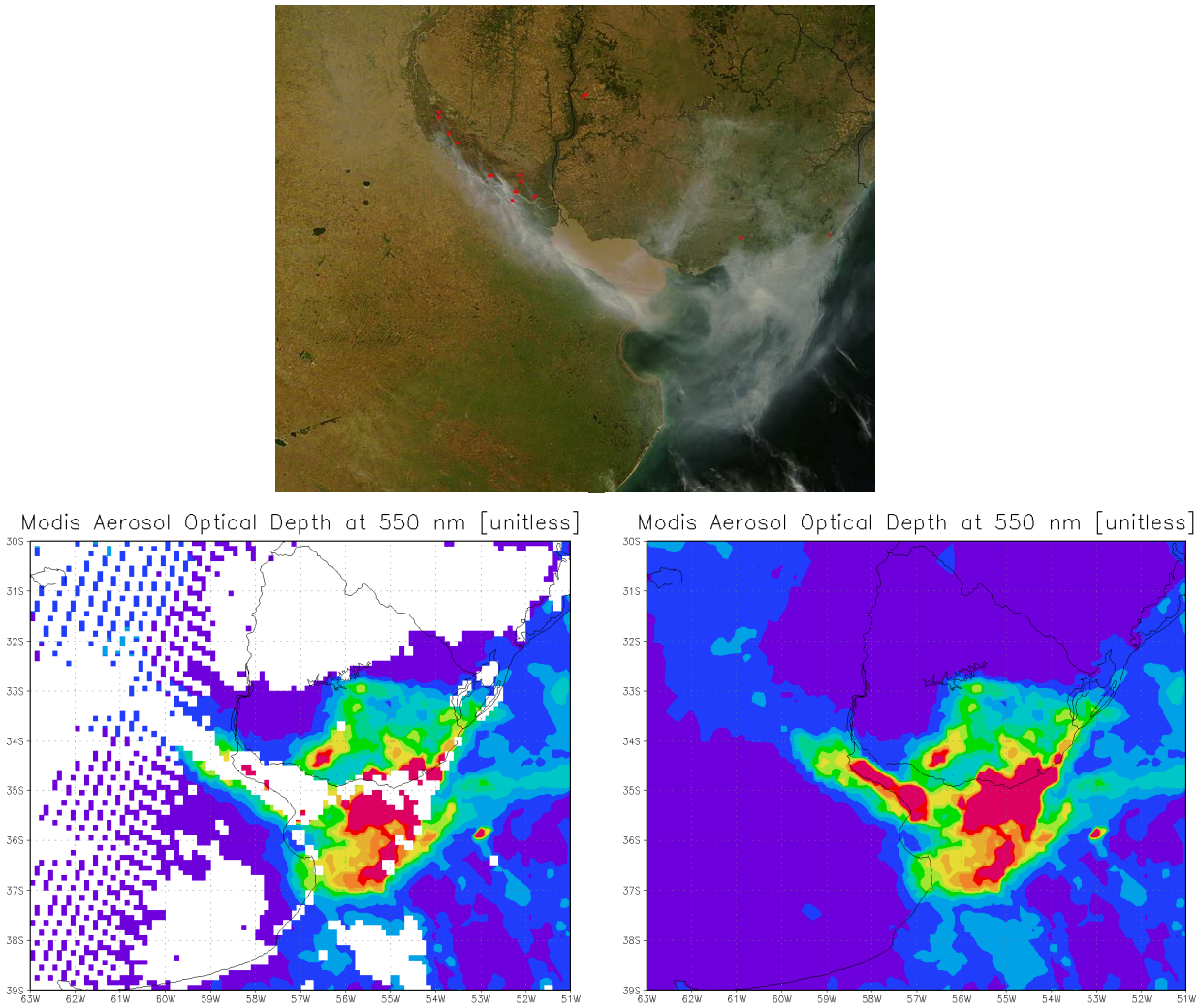

Figure 14: MODIS real-color image from TERRA on April 18 (top), and its AOT derived product (bottom). On the second panel an algorithm for interpolating missing data pixels was used.

7. ACKNOWLEDGEMENTS

This research was partially supported by research grants PIP0772 from Consejo Nacional de Investigaciones Cientificas y Técnicas (CONICET) of Argentina and PICT 2008-1417 from Agencia Nacional de Promoción Científica y Tecnológica (ANPCyT) of Argentina.

The authors are grateful to Matías Armanini, Lic. Martina Suaya, José Ares, Gerardo Lascala, and Lic. Ximena Calle from the SMN for providing the Eta/SMN model forecasts, observation data from meteorological stations, and satellite imagery from GOES-12.

MODIS real-time satellite images and fire maps are courtesy from The MODIS Rapid Response System (http://lance.nasa.gov/imagery/rapid-response/; http://rapidfire.sci.gsfc.nasa.gov/firemaps/) and from the 'Banco de Dados Queimadas' from CPTEC-INPE, Brazil (http://www.dpi.inpe.br/proarco/bdqueimadas/; http://sigma.cptec.inpe.br/queimadas/)

The program for smoke plume digitization ImageJ is courtesy from the National Institutes of Health (http://rsb.info.nih.gov/ij/index.html)

This work is based on J. Blanco's graduation thesis at the Department of Atmospheric and Oceanic Sciences from University of Buenos Aires (Blanco, 2011).

8. REFERENCES

Berbery, E., Ciappesoni H., Kalnay E., 2008: The smoke episode in Buenos Aires, 15-20 April 2008. Geophys. Res. Let, 35, L21801.

Berri, G.J., 1987: Estudio del comportamiento termohidrodinámico de la capa límite atmosférica sobre el Río de La Plata y sus inmediaciones, mediante un modelo de simulación numérica, Tesis Doctoral, Departamento de Ciencias de la Atmósfera y los Océanos, Facultad de Ciencias Exactas y Naturales, UBA, 1987.

Berri, G.J., 2009: Improving low-level wind field forecast over coastal regions with a mesoscale boundary layer model forced with local observations and regional operative forecasts, examples of lagrangian trajectories, 30th NATO/SPS International Technical Meeting on Air Pollution Modelling and its Application, San Francisco, May 2009.

Berri, G.J., Sraibman, L., Tanco R. A. and Bertossa G., 2010: Low-Level Wind Field Climatology over the La Plata River Region Obtained with a Mesoscale Atmospheric Boundary Layer Model Forced with Local Weather Observations. Journal of Applied Meteorology, 49, 1293-1305 pp.

Blanco J., 2011: Desarrollo de un modelo simplificado para el estudio de dispersión de plumas de humo por quema de pastizales, y metodología para la validación con imágenes satelitales. Tesis de Licenciatura en Ciencias de la Atmósfera, Facultad de Ciencias Exactas y Naturales, Universidad de Buenos Aires, Sep 2011.

Blanco J. and Berri G., 2010: Desarrollo de un modelo híbrido de trayectorias lagrangianas y dispersión atmosférica en alta resolución, aplicado al estudio de la contaminación del aire. Actas XXV Reunión Científica de la AAGG, Córdoba, Argentina, Nov 2010.

Blanco J., Berri G., Salles M.A., Ramis V. and Tanco R, 2010: Validación de la distribución espacial de plumas contaminantes simuladas con un modelo de dispersión atmosférica acoplado a un modelo de capa límite en mesoescala. Actas XXV Reunión Científica de la AAGG, 2010, Córdoba, Argentina, Nov de 2010.

Black, T. L., 1994: The new NMC mesoscale Eta Model: Description and forecast examples. Wea. Forecasting, 9, 265–278.

Briggs, G.A., 1972: Discussion: chimney plumes in neutral and stable surroundings, Atmos. Envir., 6:507-510.

Clements C.D and co-authors, 2007: Observing the dynamics of wildland grass fires: FireFlux – a field validation experiment. Bulletin of the American Meteorological Society 88(9), pp.1369-1382.

Gifford F., 1976: Turbulent Diffusion Typing Schemes. AReview, Nucl. Saf., 17: 68-86.

Marcuzzi E. A. and Hoevel R., 2009: Condiciones Meteorológicas en torno a los incendios ocurridos en el delta del Paraná durante el mes de abril de 2008. Actas del X Congreso Argentino de Meteorología (CONGREMET X), Buenos Aires, Oct 2009.

Mattio C. A., 2009: Combinación de herramientas para el monitoreo y seguimiento de humo generado por incendios forestales y de pastizales en la República Argentina. Actas del X Congreso Argentino de Meteorología (CONGREMET X), Buenos Aires, Oct 2009.

Mesinger F., 1984: A blocking technique for representations of mountains in atmospheric models. RI. Meteor. Aeronaut., 44, 195-202.

Mesinger F. and Z. I. Janjic, 1990: Numerical methods for the primitive equations. Ten years of Medium-Range Weather Forecasting. Reading, United Kingdom, ECMWF, 205-251.

Otero L.A. and coauthors, 2009: Humo en Buenos Aires, abril 2008. Actas del X Congreso Argentino de Meteorología (CONGREMET X), Buenos Aires, Oct 2009.

Pasquill, F., 1961: The estimation of the dispersion of windborne material. The Meteorological Magazine, vol 90, No. 1063, pp 33-49.

Rolph, G. D., and Coauthors, 2009: Description and verification of the NOAA Smoke Forecasting System: The 2007 fire season. Wea. Forecasting, 24, 361–378.

Ruminski, M., S. Kondragunta, R. Draxler, and J. Zeng, 2006: Recent changes to the Hazard Mapping System. 15th Internacional Emission Inventory Conf.: Reinventing Inventories—New Ideas in New Orleans, New Orleans, LA, EPA (http://www.epa.gov/ttn/chief/conference/ei15/session10/ruminiski.pdf).

Ruminski, M., S. Kondragunta, R. Draxler and G. Rolph, 2007: Use of environmental satellite imagery for smoke depiction and transport model initialization.16th Annual International Emission Inventory Conf.: Emission Inventories—Integration, Analysis, and Communications, Raleigh, NC, EPA (http://www.epa.gov/ttn/chief/conference/ei16/session10/ruminski.pdf).

Sraibman, L., and G. J. Berri, 2009: Low level wind forecast over La Plata River region with a mesoscale boundary layer model forced by regional operational forecasts. Bound.-Layer Meteor., 130, 407–422.